Microscopic details of the integer quantum Hall effect in an anti-Hall bar

Christoph Uiberacker,[*] Christian Stecher, and Josef Oswald
Institute of Physics, University of Leoben, Franz-Josef-Strasse 18A, 8700 Leoben, Austria
(Received 23 December 2011; revised manuscript received 25 April 2012; published 9 July 2012)

Due to the lack of simulation tools that take into account the actual geometry of complicated quantum Hall samples there are lots of experiments that are not yet fully understood. Already some years ago Mani recorded a shift of the Hall resistance transitions to lower magnetic fields in samples of a Hall bar with an embedded anti-Hall bar by using a partial gating. We use a nonequilibrium network model to simulate this geometry and find qualitative agreement. Fitting the simulated resistance curves to the experimental results we can not only determine the carrier concentration but also obtain an estimate of the screened gating potential and especially the amplitude and length scale of potential fluctuations from charge inhomogeneities which are not easily accessible by experiment.

DOI: 10.1103/PhysRevB.86.045304 PACS number(s): 73.43.Cd, 73.22.−f, 73.43.Qt

I. INTRODUCTION

The main application of the classical Hall effect lies in the simultaneous determination of the carrier concentration and the mobility. For low enough temperatures and pure samples quantum effects become important. In the quantum Hall regime experimental results for magnetic fields corresponding to plateau transitions depend on microscopic details such as the potential landscape, which complicates interpretation.

For quantum Hall effect (QHE) experiments a fixed voltage or current is applied to two metallic contacts, while additional contacts are used to measure longitudinal and transversal potential differences. For interpretation it is therefore essential to know the distribution of the electrochemical potential (ECP, to distinguish it from potentials in equilibrium) in the sample. Generic properties of the ECP have been analyzed for simple geometries in a series of papers.[1–3] The plateaus of the transversal (Hall) resistance at integer fractions $1/j$ ($j = 1,2,3\dots$) of h/e^2 as a function of magnetic field could be explained in terms of a simple modification of the Landauer model by Büttiker,[4,5] using noninteracting electrons in an empirical confinement potential.[6] However, the resistance between plateaus depends on the detailed geometry, the electrostatics of electrons, or the potential landscape generated by excess charges in the doped semiconductors in the vicinity of the 2-dimensional electron gas (2dEG).

Electrostatics was investigated self-consistently in simple geometries[2,7] and was shown to lead to the formation of alternating compressible and incompressible stripes. One concludes that in the plateau regime, current in response to (transversal) electric field only flows in the incompressible stripes. The picture becomes more complicated for nonideal contacts due to potential barriers or when applying gatings because channels are (partially) blocked and the ECP is changed in their surroundings. Dahlem *et al.* found experimentally that width and magnetic field values of the transition region between plateaus can change significantly.[8] At the same time we investigated such situations with the nonequilibrium network model (NNM),[9,10] with good agreement with the experiments.

In addition the NNM has proven successful for exotic sample geometries such as anti-Hall bars within Hall bars[11] supplied by multiple constant current sources when compared to experiments of ungated samples by Mani.[12,13] Shortly after, Mani applied partial gating to his samples and recorded a shift of the Hall resistance transitions to lower magnetic fields as a function of the gating voltage.[14] In the present paper we describe simulations of these samples with the NNM and show that the features in the experiment are well reproduced.

Moreover, by manually fitting the transversal resistance we extract the electron concentration, the screened gating potential, and the average curvature of saddle points of the electrostatic potential from charge fluctuations (e.g., by disorder). From the curvature and a statistical model we obtain independent estimates for the amplitude and length scale of this potential.

II. THEORY

The exact Hamiltonian of a typical integer quantum Hall sample is complicated due to the interface of two semiconducting layers, excess charges, and the presence of confinement as well as metallic contacts at the borders of the 2dEG. Using an effective single particle description (mean-field approximation) we write for the Hamilton operator

$$H_s = T + V_{\text{coul}} + V_g^0, \quad \nabla^2 V_{\text{coul}}(\mathbf{r}) = -4\pi e^2 \delta\rho_{mb}(\mathbf{r}), \quad (1)$$

where the (single particle) potential is a sum of a bare gate potential V_g^0 and the (self-consistent) Coulomb potential V_{coul}. The latter can be split into a Coulomb interaction in a hypothetical infinite 2dEG, using an effective local excess charge density $e\delta\rho_{mb}(\mathbf{r})$ that reflects the many-body interaction of charges, and a confinement potential V_{conf} due to edges and metallic contacts in the QHE bar. T denotes the kinetic energy operator, which is $T = \hbar\omega_c a^\dagger a$, with a the destruction operator in the Landau level (LL) basis.

For sufficiently high magnetic field, electron wave functions are highly confined to the magnetic length $l_B = \sqrt{\hbar/eB}$, where e and B denote elementary charge and magnetic induction normal to the 2dEG. Therefore electronic states are spatially localized on a network of semiclassical trajectories, which are equipotential contours in the long-range part V_{coul}^l of V_{coul}. The short-range part V_{coul}^s of V_{coul} is well described by a Gaussian density of states (DOS) for each LL, as derived by Ando.[15] We use a constant broadening of $\sigma_0 = 0.5\ (\text{meV/T})^{1/2}$ to mimic this effect. $V^l_{\rm coul}$ determines the central energy E_n of LL bands. In addition, equilibration among edge channels is taken into account by assuming tunneling in terms of an exponential function with decay parameter.

We use a simple self-consistent Thomas-Fermi approximation for zero temperature to obtain $V^l_{\rm coul}$. In spite of the slow variation of $V^l_{\rm coul}$ we use

$$\rho = n\left[B, E_f(B) - \left(V^0_g - V^l_{\rm coul}\right)\right], \quad n(B,E_f) := n_0 B \sum_j^{LL} \int_{-\infty}^{E_f} dE \exp\left(-\frac{(E-E_j)^2}{\sigma_0^2 B}\right), \quad (2)$$

where the bulk electron density, $\rho_0 = n(B,E_f(B)) = \rho_b$ (to be fitted to experiment) is equal to the density ρ_b of positive background charges and defines the Fermi energy $E_f(B)$ implicitly. The complementary equation is provided by the Poisson equation $\nabla^2 V^l_{\rm coul} = -4\pi\delta\rho$ (units of $e = 1$), with the excess charge defined as $\delta\rho := \rho - \rho_b$. The solution can be expressed in terms of the Green's function in an infinite 2D system as[16]

$$V^l_{\rm coul}(\mathbf{r}) = -2\int d\mathbf{r}' \ln|\mathbf{r}-\mathbf{r}'|\delta\rho(\mathbf{r}') \approx 4\pi\delta\rho(\mathbf{r})\int_{r_s}^{r_D} dx\, x \ln x. \quad (3)$$

Here we approximated $\delta\rho(\mathbf{r})$ as slowly varying and $r_s := 1/\sqrt{\pi\rho_0}$ is the interparticle distance while r_D denotes the screening length. Averaging over $\mathbf{r}$ gives $V^l_{\rm coul} = C\delta\rho$ with $C \approx 2\pi r_D^2 \ln r_D^{-1} eVm^2$ when r_D is inserted in units of m. We used $C = 50$ for energy in meV and density in 10^{11} cm^{-2}, which corresponds to a realistic order of magnitude of $r_D \approx 250$ nm.

Transport in high magnetic field can be viewed as a percolation problem, where it is well known that only pivotal edges are relevant to the (bond) percolation problem.[17] These edges correspond to saddle points of the potential landscape. The most prominent of this type of models is the Chalker-Coddington model,[18] which is able to predict statistics of states and scaling exponents but cannot describe the nonequilibrium steady state (which is a distribution of ECPs). In contrast, our NNM is designed to calculate these nonequilibrium quantities. The model rests on the local equilibrium approximation,[19] which is applied to a network of semiclassical wave functions. In this way we attribute unique thermodynamical quantities such as the ECP to each single wave function. Calculations of the ECP and current distribution of the classical nonequilibrium steady state of electrons and positive donors (without other dissipative mechanisms) on a microscopic (*ab initio*) level have recently been achieved.[20] The ECP distribution resembles the one in the plateau transition regime of the NNM[9] but does not yield the distribution for the resistance plateaus as expected.

Regarding the ECP and current distribution, there is a long history of random resistor networks to study conduction in disordered media.[21,22] It was noted that the usual (two-terminal) resistors cannot be used for calculating conductivity in the presence of a magnetic field, as the conductivity tensor is not globally diagonalizable. The usual approach uses 6(4)-terminal units in 3d(2d) systems together with appropriate Kirchoff rules.[23,24]

In the NNM, at each saddle of $V^l_{\rm coul}$ 4 trajectories meet, with their respective ECPs. We assume that phases are destroyed by decoherence, such that the distances between saddles become irrelevant. This resembles classical resistor networks.[23] Furthermore, it gets support from a very recent paper that shows the validity of Ohm's law well below the μm scale in dopand wires in Si using phosphorus scatterers.[25] Similar to the classical case the distance between tunneling regions (that is, generalized, multiterminal "resistor" units) is irrelevant in case of phase destruction. Therefore we can replace $V^l_{\rm coul}$ by the model potential $V(x,y) = V[\cos(\omega y) - \cos(\omega x)]$ of a regular grid of saddle points, where the period $L := 2\pi/\omega$ and amplitude V should be understood as average properties of $V^l_{\rm coul}$ that we determine by fitting to the experiment. In the same way, V_{conf} is assumed to be zero in the center of the sample and to increase quadratically a given distance from the edges to a high enough value to make the charge density practically zero at the edge.

Next we define the ratio of longitudinal to transversal field component at a saddle point as

$$P := \frac{E_x}{E_y} = \frac{u_1 - u_2}{u_1 - u_4} = \frac{u_4 - u_3}{u_2 - u_3}. \quad (4)$$

In this way we construct a "transfer" equation for the ECPs

$$\begin{bmatrix} u_2 \\ u_3 \end{bmatrix} = \begin{bmatrix} 1-P & P \\ -P & 1+P \end{bmatrix} \begin{bmatrix} u_1 \\ u_4 \end{bmatrix}. \quad (5)$$

We neglect nonlinear effects; that is, the values of P do not depend on the ECPs. This should be well justified in the case of the experimental currents of 5 nA,[14] corresponding to a voltage differences lower than 0.2 mV per LL across the sample or energies well below the Landau level (LL) spacing of $\hbar eB/m^* \approx 1.728$ meV at $B = 1$ T. The ECP distribution can be calculated as a boundary value problem once the values for P at each node are given. We model external contacts, which supply current to the NNM, by saddles with a pair of trajectories that point into/out of the sample. The ECP at one trajectory is fixed to the value of the contact, while the other is determined.

Except in a small region around the highly localized hot spots (at opposite edges of the current inducing contacts) the local conductance tensor can be approximated as purely off-diagonal. This leads immediately to $P = I_y/I_x$. This approximation produces only a small local error near the hot spot without influence on the global ECP distribution and has the advantage that only the electric field has to be calculated. According to the edge channel picture we call T the probability of transmission in the longitudinal direction; therefore we get $I_y \propto R$ and $I_x \propto T = 1 - R$. P can then be calculated from elastic tunneling transition probabilities at the Fermi energy across a saddle as[26,27]

$$P = \delta_{mn}\frac{R_{mn}}{1 - R_{mn}} = \exp\left[-\epsilon\frac{B}{c}\right], \quad (6)$$

with $\epsilon := E_F - E_n - V_S$ the energy of the trajectory, in terms of the difference of the Fermi energy to the energy of LL n, relative to the saddle (potential) energy $V_S = V^l_{\rm coul} + V_{conf}$. We define the "center of the transition" as $\epsilon = 0$. While B denotes the magnetic field strength, the parameter $c := hV/eL^2$ is related to the curvature of the model potential energy fluctuations with amplitude V. Similar to other approaches[3,28] we calculate longitudinal and transversal resistance from the ECP distribution by identifying the current with the macroscopic current direction, that is, dividing ECP differences by total current.

III. RESULTS

A. Transversal resistance and fit of experiment

Figure 1 schematically shows the geometric setup of an anti-Hall bar embedded in a Hall bar, used in the experiment.[14] The gated rectangular region is filled with yellow color and a confinement potential develops near the inner and outer border of the 2DEG, indicated by solid lines. In the experiment a constant inner/outer current was driven through the device by applying appropriate voltage differences at the contact pairs A-B of the outer Hall bar and 1-2 of the inner anti-Hall bar. We denote in the following the longitudinal (parallel to direction A-B) and transversal direction by x and y, respectively. Transversal Hall resistances R_{xy} are obtained from F-C and 6-3. As discussed in Ref. 9 it is sufficient to use point contacts in simulations of macroscopic Hall samples, such as in the present experiments.

We manually fit our simulations to the experimental results in order to obtain important microscopic information such as the carrier concentration, the enhancement factor for the Zeeman energy, the screened gating potential, and the magnitude and correlation length of the potential fluctuations. We estimate errors from half the thickness of lines in plots of the experimental results as no error bars are given.

To get the carrier concentration we fit the plateau transition center of R_{xy} of the outer ungated Hall system for the (3 last integer) transitions from fill factor $\nu = 4$ to $\nu = 3$, $\nu = 3$ to $\nu = 2$, and $\nu = 2$ to $\nu = 1$. This results in a carrier concentration of $\rho_0 = 1.81 \times 10^{11} \pm 0.02 \times 10^{11}$ cm^{-2}. Our value is slightly below the range 2×10^{11} cm$^{-2} \leqslant \rho_0 \leqslant 3 \times 10^{11}$ cm^{-2} proposed in the experimental work,[29] where however a fit to the classical Hall slope is normally used.

Due to spin polarization a Zeeman term adds to the energy, resulting in an energy difference of $\Delta E_Z = g\mu B/2$, with g an enhancement factor and $\mu := g_{\mathrm{GaAs}}\mu_B$. Here $g_{\mathrm{GaAs}} = -0.44$ is the Landé factor of GaAs heterostructures and $\mu_B = e\hbar/2m^*$ the Bohr magneton for electrons with effective

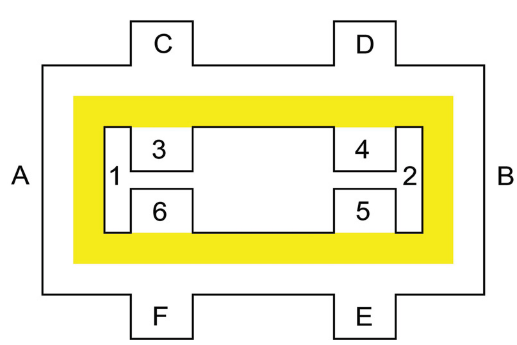

FIG. 1. (Color online) Geometry of the anti-Hall bar within a Hall bar: The figure shows the labeling of contacts used and the shaded, yellow area denotes the partial gating applied by a top gate in the experiment.

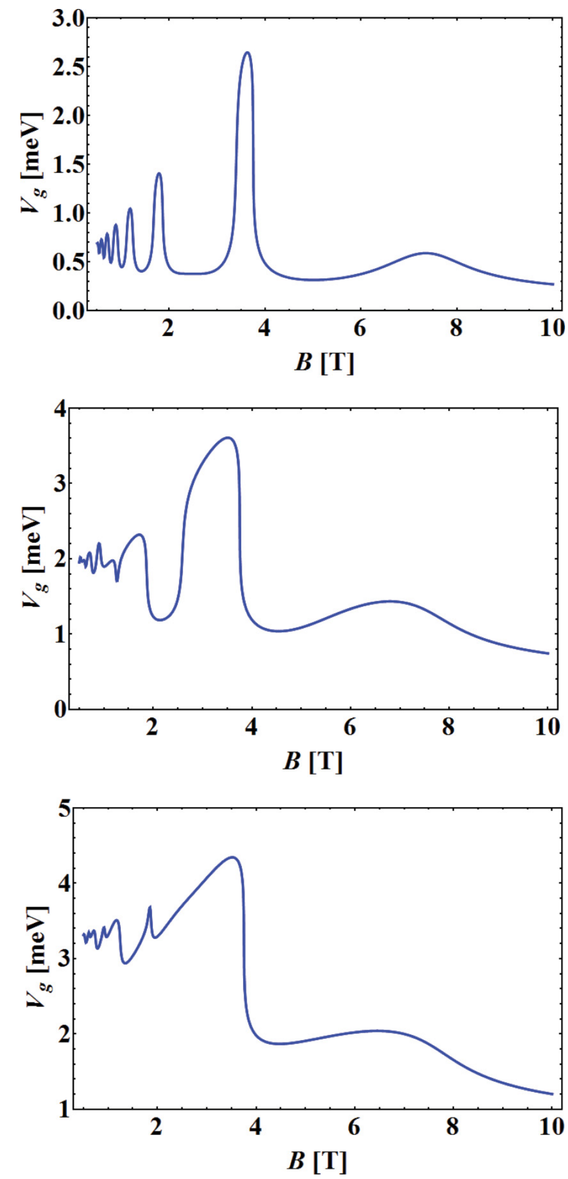

FIG. 2. (Color online) Screened gating potentials as a function of magnetic field: We show results for bare gatings of 10 meV, 30 meV, and 50 meV. Low/high screening does not directly correspond to transition/plateau regions of R_{xy} as broadened LLs for different spin significantly overlap for the Zeeman energy found.

mass m^*, which we set to the typical effective mass of GaAs, $m^* = 0.067$ m. By manually fitting the transition centers in the case of no gating we arrive at $g = 12.5 \pm 1.5$. Such large enhancement values are typically seen in transport measurements.[30]

We fit the magnetic field at the center of the plateau transitions observed in the inner and outer leg of the anti-Hall structure, and arrive at bare gating potentials of 10 meV, 30 meV, and 50 meV. The screened gating potentials $V_g(B)$ as functions of the magnetic field B are shown in Fig. 2 for these bare gating potentials. We note that within the plateau transition V_g is small and fairly constant only for small values of V_g^0. The magnetic fields at the transition centers are then collected in Table I.

TABLE I. Magnetic fields in T of the transition centers for various bare gating potentials. We estimate the error as 0.05 T.

Transition	$V_g^0 = -450$ mV	$V_g^0 = -300$ mV	$V_g^0 = -150$ mV	$V_g^0 = 0$ mV
$2 \to 1$	2.83	4.00	4.90	5.05
$3 \to 2$	1.55	2.19	2.72	2.93
$4 \to 3$	1.24	1.70	2.20	2.26

Figure 3 shows R_{xy} for various V_g^0 applied to the inner Hall bar. The dominant feature of gating lies in a shift of the plateau transitions to lower magnetic fields due to a reduced electron concentration. We remind the reader that the Fermi energy is fixed by a reservoir and therefore only a function of the magnetic field but not the local gating. The impression of a more or less rigid shift is a consequence of $E_f(B) - V_g(B)$ having small variations on the scale of the magnetic field interval of R_{xy} transitions. We mention that if the gating is large enough, which is the case for $V_g^0 = 50$ meV, the center can jump down to the next lower linear increasing part of the Fermi energy, corresponding to the neighboring LL band at lower energy (see Fig. 4).

In order to obtain the potential curvatures for all gate potentials, we would have to fit the slope at each transition for each V_g^0 separately, which is very demanding. Therefore we determine c_0 by comparing experimental curves of gated samples to our ungated R_{xy} curve and calculate from it the respective value c_v for nonzero V_g^0. We focus on the three transitions with lowest fill factor ν, starting with the center at the highest magnetic field and ordered due to decreasing magnetic field [corresponding to the states $(\nu,s) \in \{(2,+),(2,-),(1,+)\}$ crossing the Fermi energy, where s is the spin orientation]. We summarize the manually fitted c_0 values as a function of V_g^0 in Table II.

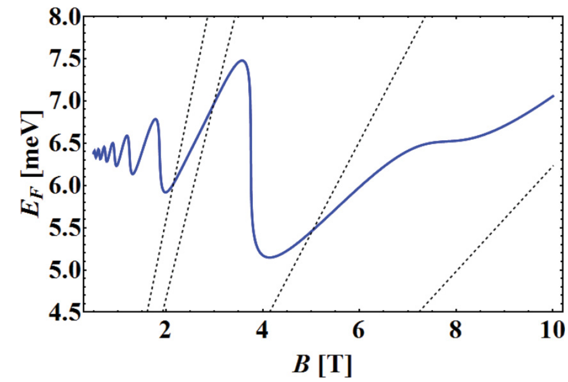

FIG. 4. (Color online) Fermi energy and 4 Landau levels of lowest energy (2 spin-resolved pairs) as functions of the magnetic field.

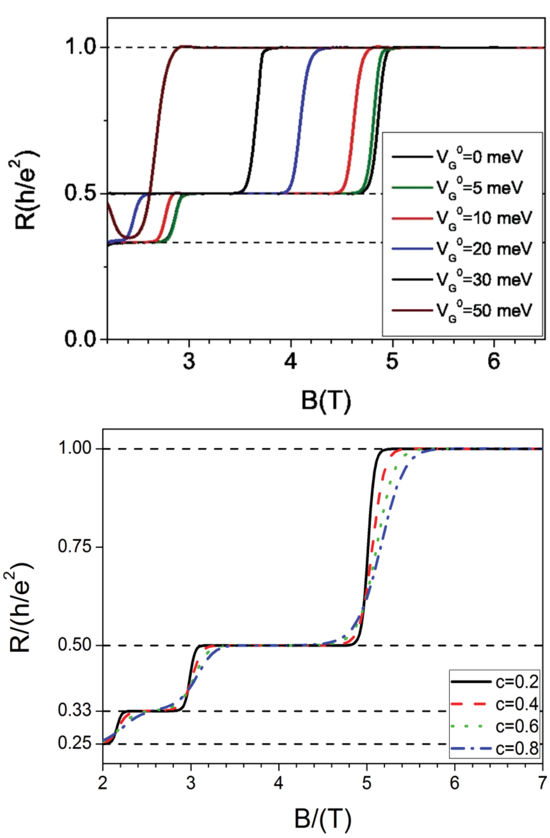

FIG. 3. (Color online) Variation of the transversal resistances as a function of magnetic field: The upper plot shows R_{xy} for various gating potentials applied to the inner gated bar. The lower curves show transversal resistance curves for various curvatures c and no gating.

It is interesting to also present the c_0 values at the leg without gating, summarized in Table III. For each transition the values should not depend on V_g^0, if there is no charge transfer from the gated to the ungated leg. It seems that the curvature decreases (the potential landscape is getting flatter) with increased gating on the opposite leg. On the other hand, we expect the charge transfer to be small in such a macroscopic bar. Within the (large) uncertainties of the experimental curves we cannot predict even a qualitative trend. Therefore we average along each row to obtain 0.17, 0.4, and 0.67 in units of meV/T for $4 \to 3$, $3 \to 2$, and $2 \to 1$, respectively.

We stress that the shift of the transition center with gating also changes the slope of R_{xy} in the center of transitions ($\epsilon = 0$) due to the appearance of B/c (note $c = a/2$, to be consistent with the definition of a in Ref. 9) in P [see Eq. (6)]. In order to compare transitions for various gatings, we demand that the interval in magnetic field δB_v, corresponding to $|\epsilon(B)B/c_v| = 1$, is the same as the one at zero gating, given by $|\epsilon(B)B/c_0| = 1$, using an appropriate definition of $c_v(c_0)$. In order to get explicit expressions we expand linearly around the magnetic field at transition centers, $\epsilon(B) \approx \epsilon_0 + \epsilon_1 B_{tr}$. In this way we

TABLE II. Fitted curvatures c_0 in units of meV/T for various transitions and bare gating potentials. We estimate the fitting error as ±0.2 meV T from the line thickness of the Hall resistance in the experimental figure.

Transition	$V_g^0 = -450$ mV	$V_g^0 = -300$ mV	$V_g^0 = -150$ mV
$2 \to 1$	0.5	0.85	1.0
$3 \to 2$	0.5	0.45	0.6
$4 \to 3$	0.3	0.4	0.2

TABLE III. Curvatures c_0 in units of meV/T for various transitions and bare gating potentials for the part of the anti-Hall bar with no gating applied.

Transition	$V_g^0 = -450$ mV	$V_g^0 = -300$ mV	$V_g^0 = -150$ mV
$2 \to 1$	0.6	0.6	0.8
$3 \to 2$	0.45	0.35	0.4
$4 \to 3$	0.1	0.2	0.2

get from $|\epsilon(B)B/c| = 1$ the interval

$$\delta B = -\frac{B_{tr}}{2} \pm \sqrt{\frac{B_{tr}^2}{4} + \frac{c}{\epsilon_1}}. \quad (7)$$

Demanding $\delta B_v = \delta B_0$ we map the two transitions onto one curve and arrive at the curvature of the gated sample,

$$c_v = \epsilon_1^v \left[-\frac{(B_{tr}^v)^2}{4} + \left(\frac{B_{tr}^v - B_{tr}^0}{2} + \sqrt{\frac{(B_{tr}^0)^2}{4} + \frac{c_0}{\epsilon_1^0}} \right)^2 \right]. \quad (8)$$

Using the values of c_0 in Table II, we calculate c_v for each transition in terms of Eq. (8), which we summarize in Table IV.

B. Potential landscape

To determine both the amplitude and length scale of the potential fluctuations we need another quantity besides the curvatures. In this respect a model of charge fluctuations by statistically independent electrons is very useful.[31,32] As is well known, if a collection of statistical objects with identical properties (described by the same random variable) are independent then the relative fluctuations of $X := \sum_j^N X_j$ are given by $\Delta X/\langle X \rangle \propto N^{-1/2}$, where $\langle X \rangle$ denotes the average of X and $\Delta X := \sqrt{\langle (X - \langle X \rangle)^2 \rangle} = [\sum_{j,k}^N \langle X_j X_k \rangle - \langle X \rangle^2]^{1/2}/N$ together with $\langle X_j X_k \rangle = \delta_{jk}$.

We partition the sample in N cells of equal size and interpret the electron distribution (or number of electrons) in each cell as a random variable. Assuming charge neutrality on the average the absolute fluctuations of the charge density n are then $\delta\rho = \rho_0/N^{1/2}$. Employing the Poisson equation we then get the estimate V [meV] $= |\frac{2\pi e 10^3}{\kappa K}\delta\rho|$ for the magnitude of the (long range) potential energy fluctuations.[31] $\kappa = 1.3797 \times 10^{-9} C/Vm$ denotes the dielectric constant of the sample (GaAs) and K is the modulus of the smallest wave vector supported by geometry.

The detailed description of the experimental setup[14] lets us estimate the length of each leg as $l = 2$ mm and the transversal

TABLE IV. Effective curvatures c_v in units of meV/T for various transitions and bare gating potentials used in the experiment.

Transition	$V_g^0 = -450$ mV	$V_g^0 = -300$ mV	$V_g^0 = -150$ mV	$V_g^0 = 0$ mV
$2 \to 1$	0.25	0.51	0.93	0.67
$3 \to 2$	0.17	0.17	0.47	0.40
$4 \to 3$	0.11	0.24	0.20	0.17

TABLE V. Number of correlated electrons in statistically independent cells. We rounded to the next higher/lower integer.

Transition	$V_g^0 = -450$ mV	$V_g^0 = -300$ mV	$V_g^0 = -150$ mV	$V_g^0 = 0$ mV
$2 \to 1$	5	5	4	4
$3 \to 2$	3	2	2	2
$4 \to 3$	2	2	2	2

width as $w = 0.2$ mm. Assuming variations of charge only normal to equipotential lines the largest wavelength should occur in the middle of the plateau transition where the Hall angle is close to $\pi/4$. We arrive at a wavelength of $2\pi/K = 2 \times 10^{-4}\sqrt{2}$ meters. Moreover we get $\delta\rho = \rho_0/\sqrt{N} = \sqrt{\rho_0 N_c/lw}$. Noting that n hardly varies between transitions we use averages for each V_g^0. The fitted densities (in 10^{-11} cm^{-2}) turn out to be $\rho_0 = 1.81$, $\rho_0 = 1.62$, $\rho_0 = 1.25$, and $\rho_0 = 0.88$ for bare gating (in meV) $V_g^0 = 0$, $V_g^0 = 10$, $V_g^0 = 30$, and $V_g^0 = 50$, respectively. N_c denotes the number of (correlated) electrons in each fictitious cell of the statistical model. The amplitudes of potential fluctuations become $V/\sqrt{N_c} = 2.203$, 1.972, 1.521, and 1.071, respectively, in units meV, for increasing gating.

This gives the interesting possibility to get a value for the number of correlated electrons, as explained in the following: A plausible upper bound for N_c is given by the energy difference between LLs, because the screening tries to suppress higher potential amplitudes due to Wulf *et al.*[31] Namely, if the potential energy exceeds the LL spacing a new LL band is occupied, which leads to strong screening that suppresses the potential until the new LL band is emptied and screening is weak again. Clearly this argument does not hold for potentials that are so large as to change the level structure significantly or lead to the breakdown regime. We arrive in this way at the upper bounds N_c^u that are presented in Table V. The variation with V_g^0 turns out to be small.

Using the definition of the curvature we get the potential correlation length in nm as

$$L = \sqrt{\frac{hV}{ec_v}} = v\sqrt{\frac{\sqrt{N_c}}{c_v}}, \quad (9)$$

where $V = ev^2\sqrt{N_c}/h$ with numerical values $v = 95.46$, 85.44, 65.93, and 46.41 for increasing gating. The so obtained potential correlation lengths are summarized in Table VI. We judge the error as coming predominantly from the curvature, because the concentration n can be fitted with high accuracy. The resulting error varies strongly due its proportionality to $c^{-3/2}$. Qualitatively the error is less for less gating and smaller fill factor (that is, for larger value of L in Table VI).

Table VI, which shows microscopic information that is hard to be addressed by experiment, is our main result. These values should be viewed as the largest correlation lengths appearing in the potential landscape, due to the Hartree-like estimation of the potential amplitude used. The general trend is decreasing screening (smaller L) with increasing V_g^0. This makes sense, despite the high error for low L, and is due to decreased carrier concentration. Similarly the screening increases with

TABLE VI. Correlation length and their errors of potential energy fluctuations in nm, using the values of N_c from Table V. Parentheses indicate values with large errors.

Transition	$V_g^0 = -450$ mV	$V_g^0 = -300$ mV	$V_g^0 = -150$ mV	$V_g^0 = 0$ mV
$2 \to 1$	138.8 ± 55.5	138.0 ± 27.1	125.3 ± 13.5	164.9 ± 24.6
$3 \to 2$	148.2 ± 87.1	(190.3 ± 111.9)	148.2 ± 31.5	179.5 ± 44.9
$4 \to 3$	(166.5 ± 151.3)	160.1 ± 66.7	227.1 ± 113.6	(275.3 ± 162.0)

the number of electrons present at transitions, that is, with decreasing magnetic field, due to the same reason. However, there are exceptions to the rule which seem to come from the nontrivial dependence of the Fermi energy and screened gating potential energy with the magnetic field.

We stress that via K a larger area of the 2dEG sample leads in principle to higher potential fluctuations, which gives different N_c due to the saturation at the LL energy difference. Furthermore, the presented (large scale) correlation lengths have a realistic order of magnitude when compared to experiments[33–35] as well as to our own Hartree-Fock (HF) calculations, using our refined version, with Broyden mixing for fast convergence, of a code originally written by Römer *et al*.[36] We note here that in reality due to imperfect screening a reminiscence of the distribution of charge from doping centers near the 2dEG affects the assumed statistical independence slightly. However, as shown by Gudmundsson *et al.*[32] the agreement with experiments is good.

C. Electrochemical Potential distribution

Finally, in Fig. 5 we present details of the ECP distribution for the case corresponding to a bare gating of $V_G^0 = 30$ meV

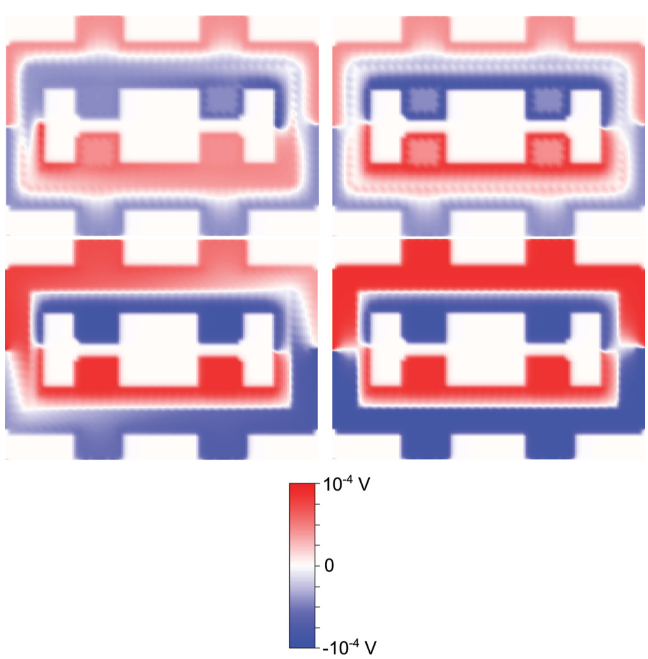

FIG. 5. (Color online) Distribution of the electrochemical potential: We show results for a bare gating potential of 30 meV and magnetic field values (from top left to bottom right) of 3.66 T, 4.20 T, 4.86 T, and 5.50 T.

(−300 mV in the experiment). We selected 4 magnetic field values to show the generic behavior. We first note that with increasing B the maximum voltage difference in the system increases, which is a consequence of constant injected current. At 3.66 T the inner (gated) bar is in the transition region, which can clearly be seen from the longitudinal gradient in blue/red color in the upper/lower leg. On the other hand the red color on the other bar is homogeneous; that is, it is in the plateau and dissipation only occurs at the current contacts. At 4.20 T the inner and outer bar are in the plateau; therefore only a transversal gradient develops and the line of zero ECP (white) is parallel to the longitudinal direction along the leg. 4.86 T shows qualitatively the same behavior as 3.66 T with the role of inner and outer bar reversed. Now the outer bar shows a longitudinal gradient. Finally at 5.50 T both bars are in the plateau again.

IV. SUMMARY AND CONCLUSION

In summary we present simulations of experiments done on an anti-Hall bar within a Hall bar geometry by Mani,[14] which show a shift of the Hall resistance to lower magnetic field by applying partial gating. We calculate the ECP distribution for the integer quantum Hall regime under a constant current condition, as used in the experiment. The so obtained transversal resistances as a function of magnetic field compare well with the experimental curves.

Fitting by hand the position of plateau transitions of the transversal resistance for applied gating, we are able to obtain the electron density, the enhancement factor for the Zeeman interaction, and the screened gating potential in the 2d electron gas. Finally we determine the curvature of potential saddles by fitting the width of plateau transitions using the ungated Hall resistance curve. Employing a model of partitioning the sample into statistically independent cells with correlated electrons in each cell, we arrive at the amplitude of potential fluctuations. Defining a transformation we obtain plateau transition intervals for the gated system from the fitted values of the ungated system. In this way we are able to provide the magnitude *and* length scale of potential fluctuations from charge inhomogeneities as a function of the fill factor of the transition and bare gating potential.

ACKNOWLEDGMENT

This work was sponsored by the Austrian Science Fund under the Research Program No. P 19353-N16.

*christoph.uiberacker@unileoben.ac.at

[1] A. H. MacDonald, T. M. Rice, and W. F. Brinkman, Phys. Rev. B **28**, 3648 (1983).
[2] D. B. Chklovskii, B. I. Shklovskii, and L. I. Glazman, Phys. Rev. B **46**, 4026 (1992).
[3] K. Güven and R. R. Gerhardts, Phys. Rev. B **67**, 115327 (2003).
[4] P. Středa, J. Kučera, and A. H. MacDonald, Phys. Rev. Lett. **59**, 1973 (1987).
[5] M. Büttiker, Phys. Rev. B **38**, 9375 (1988).
[6] S. Datta, *Electron Transport in Mesoscopic Systems* (Cambridge University Press, Cambridge, 1995).
[7] A. Siddiki and R. R. Gerhardts, Phys. Rev. B **68**, 125315 (2003).
[8] F. Dahlem, E. Ahlswede, J. Weis, and K. v. Klitzing, Phys. Rev. B **82**, 121305 (2010).
[9] C. Uiberacker, C. Stecher, and J. Oswald, Phys. Rev. B **80**, 235331 (2009).
[10] J. Oswald and M. Oswald, J. Phys.: Condens. Matter **18**, R101 (2006).
[11] M. Oswald, J. Oswald, and R. G. Mani, Phys. Rev. B **72**, 035334 (2005).
[12] R. Mani, J. Phys. Soc. Jpn. **65**, 1751 (1996).
[13] R. G. Mani, Europhys. Lett. **36**, 203 (1996).
[14] R. Mani, Appl. Phys. Lett. **70**, 2879 (1997).
[15] T. Ando, A. B. Fowler, and F. Stern, Rev. Mod. Phys. **54**, 437 (1982).
[16] G. Hellwig, *Partial Differential Equations* (B. G. Teubner, Stuttgart, 1977).
[17] G. Grimmett, *Percolation* (Springer, Berlin, 1999).
[18] J. T. Chalker and P. D. Coddington, J. Phys. C **21**, 2665 (1988).
[19] D. N. Zubarev, *Nonequilibrium Statistical Thermodynamics* (Plenum Publishing Corporation, New York, 1974).
[20] T. Kramer, V. Krueckl, E. J. Heller, and R. E. Parrott, Phys. Rev. B **81**, 205306 (2010).
[21] A. Miller and E. Abrahams, Phys. Rev. **120**, 745 (1960).
[22] S. Kirkpatrick, Rev. Mod. Phys. **45**, 574 (1973).
[23] A. K. Sarychev, D. J. Bergman, and Y. M. Strelniker, Phys. Rev. B **48**, 3145 (1993).
[24] Y. M. Strelniker, R. Berkovits, A. Frydman, and S. Havlin, Phys. Rev. E **69**, 065105 (2004).
[25] B. Weber, S. Mahapatra, H. Ryu, S. Lee, A. Fuhrer, T. C. G. Reusch, D. L. Thompson, W. C. T. Lee, G. Klimeck, L. C. L. Hollenberg *et al.*, Science **335**, 64 (2012).
[26] H. A. Fertig and B. I. Halperin, Phys. Rev. B **36**, 7969 (1987).
[27] M. Büttiker, Phys. Rev. B **41**, 7906 (1990).
[28] G. Nachtwei, Physica E **4**, 79 (1999).
[29] R. G. Mani, Phys. Rev. B **55**, 15838 (1997).
[30] T.-Y. Huang, Y.-M. Cheng, C. T. Liang, G.-H. Kim, and J. Y. Leem, Physica E **12**, 424 (2002).
[31] U. Wulf, V. Gudmundsson, and R. R. Gerhardts, Phys. Rev. B **38**, 4218 (1988).
[32] V. Gudmundsson and R. R. Gerhardts, Phys. Rev. B **35**, 8005 (1987).
[33] K. L. McCormick, M. T. Woodside, M. Huang, M. Wu, P. L. McEuen, C. Duruoz, and J. S. Harris, Phys. Rev. B **59**, 4654 (1999).
[34] P. Weitz, E. Ahlswede, J. Weis, K. V. Klitzing, and K. Eberl, Physica E **6**, 247 (2000).
[35] E. Ahlswede, P. Weitz, J. Weis, K. Von Klitzing, and K. Eberl, Physica B **298**, 562 (2001).
[36] R. A. Römer and C. Sohrmann, Phys. Status Solidi B **245**, 336 (2008).